Farooq, M.U. et al. (2008) *EBSD mapping of herringbone domain structures in tetragonal piezoelectrics.* Journal of Applied Physics, 104 . 024111. ISSN 0021-8979

http://eprints.gla.ac.uk/5934/

Deposited on: 02 June 2009

Enlighten – Research publications by members of the University of Glasgow
http://eprints.gla.ac.uk

EBSD mapping of herringbone domain structures in tetragonal piezoelectrics

M.U. Farooq[1], R. Villaurrutia[1], I. MacLaren[1], T.L. Burnett[2], T.P. Comyn[2], A.J. Bell[2], H. Kungl[3], M.J. Hoffmann[3]

[1]*Department of Physics and Astronomy, University of Glasgow, Glasgow G12 8QQ, UK*

[2]*Institute for Materials Research, University of Leeds, Leeds LS2 9JT, UK*

[3]*IKM, Universität Karlsruhe, Haid-und-Neu-Str. 7, 76131 Karlsruhe, Germany*

Herringbone domain structures have been mapped using electron backscatter diffraction (EBSD) in two tetragonal piezoelectrics, lead zirconate titanate, $Pb(Zr,Ti)O_3$, and bismuth ferrite – lead titanate, $(PbTi)_{0.5}(BiFe)_{0.5}O_3$. Analysis of the domain misorientations across the band junctions shows that the structures correspond very well to crystallographic models. High resolution mapping with a 20 nm step size allowed the crystal rotation across one of these band junctions in lead zirconate titanate to be studied in detail and allowed an improved estimation of the peak strain at the junction, of 0.56 GPa. The significance of this for crack nucleation and propagation in such materials is discussed.

I. INTRODUCTION

Piezoelectric materials are a vital part of our modern world whether in established applications as transducers and actuators or in more recent developments such as ferroelectric random access memories. It is well known that such materials display a domain structure in order to reduce both macroscopic strains and

macroscopic polarisation. Additionally, the form of the domain structure tends to be such that microscopically both large elastic strains and free charges (head-to-head or tail-to-tail polarisation) are avoided where possible. In the case of tetragonally distorted perovskites such as Ti-rich lead zirconate titanate; the domains tend to form lamellar arrangements with the boundaries on {101} planes. At these boundaries, the polarisation axis rotates by an angle of close to 90° about a <010> direction, thus the common title of 90° domain boundaries; the actual angle, 90°-α given by $2\tan^{-1}(a/c)$[1].

In a macroscopic arrangement, all three possible orientations of the [001] axis need to be present to minimise the long-range strain resulting from the ferroelectric transformation, and this imposes the requirement of a more complex structure containing different lamellar bands or colonies within the same grain; in large-grained materials this often results in the formation of the so-called herringbone structure where two lamellar bands meet; this has been discussed in detail by Arlt and Sasko[2]. Unfortunately, the junctions between the different lamellar structures are inevitably strained, and must therefore act as stress concentrations[1-7]. Our initial research on this made some simplistic estimates of the stresses present based on transmission electron microscopy imaging and diffraction and showed that high stresses may be present which could influence both the piezoelectric properties (making the material piezoelectrically hard by impeding domain movement) and the fatigue susceptibility of this material under extended use. The present study concerns the detailed structure of such herringbone junctions in two different materials using EBSD, how this compares with crystallographic models, and how the resulting information can be used to gain improved estimates of the stress concentrations at the junctions.

II. EXPERIMENTAL

$(BiFeO_3)_{0.50}$-$(PbTiO_3)_{0.50}$ (BFPT) single crystals were grown using the flux method. A platinum crucible containing the charge of a stoichiometric composition of BFPT mixed in a ratio of 60% BFPT composition: 40% $(PbO)_{0.70}$-$(Bi_2O_3)_{0.30}$ flux was sealed in an alumina crucible. Following heating to 1200°C the batch was cooled at a rate of 2°C per hour to 800°C, after which the cooling proceeded at 50°C per hour. The crystals were removed from the flux after leaching with acetic acid; more details of the preparation method are provided elsewhere[8]. The crystals were embedded in epoxy resin before grinding flat using 600, 1200 and 2500 grit silicon carbide, prior to polishing with 6μm and then 1μm diamond paste, and final fine polishing using a colloidal silica suspension.

Lead zirconate titanate 42.5/57.5 ($PbZr_{0.425}Ti_{0.575}O_3$) PZT ceramics doped with 1 mol. % La and 2 mol. % Sr were made by a conventional mixed oxide preparation technique from PbO, ZrO_2 and TiO_2, La_2O_3 and $SrCO_3$ and sintered at 1225°C for 2 hours under an oxygen atmosphere. Fuller details of the preparation method are given by Hammer and Hoffmann[9]. The samples for microstructural investigations of PZT material were prepared by sectioning the sintered cylindrical bodies of the material vertically, thus exposing the interior surface of the material. Specimens for EBSD were ground on 1000 grit silicon carbide papers and polished using 6 and 3 μm diamond paste and 1 and 0.25 μm alumina suspension, followed by a final polish with colloidal silica to remove strains and provide a high quality surface finish. A final light etch of 100 ml H_2O, 5 ml HCl and five drops HF was applied for 9 seconds to reveal a small amount of domain topography. Both the PZT and the BFPT materials were finally prepared for scanning electron microscope (SEM) observation and

electron backscatter diffraction (EBSD) by coating them with a thin coat of carbon to minimise charging.

Backscattered electron images of the BFPT materials were recorded with a solid-state detector mounted below the pole piece on a LEO 1530 Gemini FEGSEM at 20kV using a 60 μm probe limiting aperture and a working distance of 6mm. Some EBSD investigations (specifically Figure 2 in this publication) were performed on the same microscope using Oxford instruments INCA software and an INCA Mk1 crystal camera using an accelerating voltage of 20kV and a working distance of 18mm.

The secondary electron images of the PZT and the majority of the EBSD data were obtained using a FEI Quanta 200F environmental SEM equipped with an EDAX Digiview II EBSD camera. For EBSD pattern acquisition the microscope was operated at 25 kV accelerating voltage and 13 mm working distance using OIM EBSD data acquisition and data analysis software from EDAX.

X-ray diffraction studies of the PZT lattice parameters were performed using a Siemens D500 diffractometer with Cu K_α radiation using an angular range from 20º to 72.5º and a step size of 0.02º.

III. RESULTS

A. Bismuth Ferrite – Lead Titanate

The $(BiFeO_3)_{0.5}(PbTiO_3)_{0.5}$ single crystal was found to have a tetragonal structure with lattice parameters approximately a = 3.88 Å and c = 4.27 Å as determined by X-ray diffraction[10], which corresponds to a c/a ratio of 1.1. The microstructure of the sample accords well with Arlt's description of such coarse

grained tetragonal ferroelectrics[2] in that the herringbone-type domain structures are widely observed, as can be seen in Figure 1a. The larger scale structure shows the persistence of such alternating bands in a herringbone fashion over hundreds of microns, as shown in Figure 1b.

When this is orientation mapped using EBSD with a large step size to cover a large area as shown in Figure 2, each lamellar band shows just one orientation but the crystal orientation of any given band differs significantly from its neighbours with a typical misorientation of 85° about an axis close to <100>.

When EBSD mapping is performed on a junction region with a much smaller step size of 80 nm then the individual lamellae are resolved and all four domains can be seen in the orientation map of Fig. 3a, which is coloured according to the inverse pole figure key of Fig. 3b. A domain boundary map from the same data is presented in Fig. 3c, where the colours in the domain boundary map correspond to the colours of bars in the misorientation angle histogram of Fig. 3d. The mean domain misorientation from the histogram is about 84º. However the misorientations between the "90º" domains are about ~ 83º to the upper right of the diagonal junction whereas to the lower right higher misorientations of ~ 84.5º are measured. The misorientation between domains 1 and 2 (different shades of green) is about 86.2º ± 0.5° about an angle close to <100> whereas the misorientation between orientations 3 and 4 was calculated to be about 7.6º around an axis averaged out as [-0.47, 0.57, 0.60], which makes an angle of 5.5° with $[\bar{1}11]$. In accordance with previous studies[11], this relatively small misorientation was associated with large errors in the measurement of the axis of up to 10°, and the misorientation axis is therefore within error limits of $[\bar{1}11]$.

B. Lead Zirconate Titanate

The lattice parameters of the La-Sr doped PZT 42.5/57.5 material were estimated from an X-ray diffractogram recorded with Cu Kα radiation by comparing the positions of the 200 and 002 peaks using a Si standard to ensure reliable calibration of the peak positions; full Rietveld refinement of the data was not considered necessary for the level of accuracy required in the lattice parameters. The parameters were measured to be a = 4.016 Å and c = 4.137 Å corresponding to c/a = 1.030.

Figure 4 is a secondary electron image of the domain structure in the PZT sample. In this sample, the grains are of the order of 5 μm in size and the domain structure within these relatively small grains is somewhat different to that observed in the BFPT sample or that shown by Arlt and Sasko[2] in their classic paper for coarse-grained $BaTiO_3$; a variety of lamellar structures are seen in each grain but well-defined herringbone structures are less apparent and the boundaries between areas with different lamellar orientations are often more irregular.

An EBSD orientation map was recorded using a large step size to cover more than one domain simultaneously and this is shown in Figure 5a. As for the BFPT, one orientation is detected predominantly for each lamellar orientation and each area appears as a solid colour (with occasional misindexing of individual points). A range of boundaries are found in this map including grain boundaries as well as boundaries of different lamellar areas within the same grain. The grain boundaries have a variety of angles, whereas lamellar areas are exclusively related by rotation angles close to 90°. Thus, a boundary map is shown Figure 5b where boundaries in the range of 87-90° (the boundaries between areas of different lamellar orientation) are given a colour

according to the colours in the misorientation histogram shown in Figure 5c and other boundaries (e.g. grain boundaries) show up as black lines. This boundary map of Figure 5b is overlaid on the pattern quality map, where the grain boundaries show up as dark areas due to the difficulty of indexing at grain boundaries due to pattern overlaps and lattice strains.

It is clear from comparing the orientation map and the boundary map that most of the larger grains display three different orientations; for instance the large grain to the lower right contains areas with reddish pink, cyan, and pale green colours. These three orientations in the larger grains correspond to the three possible orientations of the c-axis within a grain. From examining the domain patterns within each individual grain, the conclusions above from the conventional SEM imaging are confirmed in that straight boundaries between different domain bands (which could correspond to regular herringbone domain structures) do not predominate although they are observed.

An SEM image of a lightly etched domain structure in shown in Figure 6 and some herringbone-like structures are apparent here, as well as contrast inversions, probably due to wandering 180° domain boundaries. One area on the boundary between two lamellar bands in the herringbone structure is arrowed and was used for a detailed EBSD mapping experiment. The junction of domains is shown magnified in Fig. 7c. An orientation map from the selected area is shown in Fig. 7a. The orientation across the *ad* and *a'd'* boundaries does not show any apparent change to the eye in this figure but detailed measurements (discussed below) show a small orientation change across the domain boundary. According to the model of Arlt and Sasko[2], these boundaries are 180° domain boundaries, but please note that EBSD is only sensitive to geometry and does not detect the sense of the c-axis (which only

shows up in diffraction patterns as subtle intensity asymmetries) so 180°-domain boundaries are not directly detected. The domain boundary map of Fig. 7b shows domain boundaries coloured according to the misorientation angles in the misorientation angle histogram of Fig. 7d. The misorientations *ab* and *cd* show a similar distribution to that reported previously for "90°" boundaries[12] about a median of 88.8º with misorientation axes of the type <100>. The misorientation of the "90°" domain boundary *bc* was found to be 89.50° ± 0.15° about an axis very close to $[\bar{1}00]$.

To study the small orientation changes across the 180° domain boundaries *ad* and *a'd'* in more detail, the data was reprocessed and the results are shown in Figure 8. Fig. 8a is a low angle grain boundary map where red lines represent "90°" domain boundaries (i.e. high misorientation angles) and yellow lines represent misorientations in the range 0.5º-1.2º (i.e. the low angle misorientations); boundaries with misorientations smaller than this were excluded to prevent the map being overwhelmed by low angle "orientation noise"[13]. Comparing Fig. 8a with Fig. 7a show that these low angle grain boundaries fall between domain *a* and *d* as well as between *a'* and *d'*, that is at the 180º domain boundaries in the structure. The misorientation across these "180°" domain boundaries was investigated in more detail by extracting line profiles of misorientation across these "180°" boundaries, which are shown by trail of green pixels in Fig. 8a. The variation of the misorientation angles along these lines is shown in Fig. 8b and 8c. According to the two figures the rotation of lattice from domain *a* and *d* and from *a'* to *d'* is about 1.04º and 0.97º over a distance of about 70 and 55 nm respectively.

IV. DISCUSSION

A. Comparison of the experimental data to crystallographic models

In our previous publications[1,12], we showed that within lamellar structures, the misorientation across the domain boundaries tended to agree with geometric models very well with a rotation of $2\tan^{-1}(a/c)$ about a <010> axis; the rotation angles tended to match well to published those expected from the lattice parameters determined by X-ray diffraction, although some local deviations may be present. This finding is reinforced by the present work. In the case of BF-PT, misorientations of about 83° and 84.5° about <010> were determined for two different lamellar structures; the former value agrees well with $\theta = 90°-\alpha = 83.2°$ calculated from published X-ray diffraction data for this composition (a = 3.88 Å and c = 4.37 Å, corresponding to c/a = 1.126[14]), whereas the latter agrees better with powder diffraction studies of this sample[10] which show a c/a ratio close to 1.10; this is clear evidence of local crystallographic inhomogeneities in this material. In the case of the PZT 42.5/57.5, a misorientation of about 88.8° about <010> is observed, showing some local deviation from the expected value of 88.3° for the XRD measured c/a ratio of 1.03 and suggesting that locally the c/a ratio is more like 1.021.

The main point of the present work is, however, to focus on the structure of the junctions between lamellar bands in the so-called "herringbone"-type structures. These have been previously discussed in an idealised form by Arlt and Sasko[2], Arlt[3], Pertsev and Arlt[6], mainly with a view to determining the excess energy stored in such structures, as well as by Mori *et al.*[7] in order to explain neutron and synchrotron diffraction profiles from herringbone structured martensite structures. More recently,

this was studied experimentally by MacLaren *et al.*[1] and consideration was given to the stress concentration in such structures. The structure of one of these four-domain structures can be better understood by reference to Figure 9; this shows the lattice rotations from one domain to its neighbours. Now, in the model of Arlt, the domain pair separated by a 180° boundary (*a* and *d* in Figure 9) will have domain widths of half of the other pair separated by a 90° boundary (*b* and *c*). Schmitt *et al.*[15] showed that this bimodality is often evident in reality although it is not normally as extreme as the 2:1 ratio suggested by Arlt. The diagram of Figure 9 shows the domain structure as clearly bimodal in domain widths.

The following analysis includes some features previously considered by MacLaren *et al.*[1] and Mori *et al.*[7] but includes more explicit consideration of the partitioning of rotational mismatches between different parts of the junction. If we assume for the sake of simplicity that all the "90°" domain boundaries have an idealised tilt angle given by $\theta = 90° - \alpha = 2\tan^{-1}(a/c)$ about a <100> axis then the three rotations *ab*, *bc*, and *cd* can be represented by:

$$\begin{aligned} ab&: \quad [010] \,/\, \theta \\ bc&: \quad [\bar{1}00] \,/\, \theta \\ cd&: \quad [010] \,/\, \theta \end{aligned} \tag{2}$$

all of which can be seen by detailed examination of Figure 9. Moreover, it is clear that although the axes in domain *d* are somewhat rotated with respect to those in domain *a* after this sequence of rotations, the axes could at least be brought back to within a small angle of their original orientations by applying a 180° rotation about a $[1\bar{1}0]$ axis (the original orientation would then be reproduced exactly if we had perfect 90° rotations).

These can all be written as matrices:

$$ab \quad \begin{pmatrix} \cos\theta & 0 & -\sin\theta \\ 0 & 1 & 0 \\ \sin\theta & 0 & \cos\theta \end{pmatrix} \tag{2}$$

$$bc \quad \begin{pmatrix} 1 & 0 & 0 \\ 0 & \cos\theta & -\sin\theta \\ 0 & \sin\theta & \cos\theta \end{pmatrix} \tag{3}$$

$$cd \quad \begin{pmatrix} \cos\theta & 0 & -\sin\theta \\ 0 & 1 & 0 \\ \sin\theta & 0 & \cos\theta \end{pmatrix} \tag{4}$$

$$[1\,\bar{1}\,0]\,/\,180° \quad \begin{pmatrix} 0 & -1 & 0 \\ -1 & 0 & 0 \\ 0 & 0 & -1 \end{pmatrix} \tag{5}$$

and these can then be multiplied to yield a matrix describing the lattice rotation from *a* to *d*:

$$ad \quad \begin{pmatrix} \sin^2\theta & -\cos\theta & \sin\theta\cos\theta \\ -\cos^2\theta + \sin^2\theta\cos\theta & \sin^2\theta & \sin\theta\cos\theta + \sin\theta\cos^2\theta \\ -\sin\theta\cos\theta - \sin\theta\cos^2\theta & -\sin\theta\cos\theta & \sin^2\theta - \cos^3\theta \end{pmatrix} \tag{6}$$

This equates to a rotation of an angle:

$$\Theta = \cos^{-1}\left(\frac{a_{11} + a_{22} + a_{33} - 1}{2}\right) = \cos^{-1}\left(\frac{3\sin^2\theta - \cos^3\theta - 1}{2}\right) \tag{7}$$

if θ is calculated from c/a, then an approximately linear relationship between c/a ratio and Θ is found, with increasing deviations from linearity as θ diverges from 90°.

The misorientation axis of *ad* may be shown to be (this is written as a column vector due to space considerations):

$$\begin{bmatrix} u \\ v \\ w \end{bmatrix} = \begin{bmatrix} -\sin\theta\cos\theta(2+\cos\theta) \\ \sin\theta\cos\theta(2+\cos\theta) \\ \cos\theta(1-\cos\theta+\sin^2\theta) \end{bmatrix} // \begin{bmatrix} -\sin\theta(2+\cos\theta) \\ \sin\theta(2+\cos\theta) \\ (2-\cos\theta-\cos^2\theta) \end{bmatrix} \tag{8}$$

These matrices and vectors are all written in a cubic Cartesian reference frame for simplicity and to transform these to the tetragonal indices, we need to multiply the *w* component of the vector by *a/c*. Now since:

$$\frac{a}{c} = \tan\frac{\theta}{2} \qquad \text{and} \qquad t = \tan\frac{\theta}{2} = \frac{1-\cos\theta}{\sin\theta} \tag{9}$$

in tetragonal coordinates:

$$\begin{bmatrix} u \\ v \\ w \end{bmatrix}_{\text{tetragonal}} // \begin{bmatrix} -\sin\theta(2+\cos\theta) \\ \sin\theta(2+\cos\theta) \\ \dfrac{(2+\cos\theta)(1-\cos\theta)^2}{\sin\theta} \end{bmatrix} // \begin{bmatrix} -1 \\ 1 \\ \dfrac{(1-\cos\theta)^2}{\sin^2\theta} \end{bmatrix} = \begin{bmatrix} -1 \\ 1 \\ (a/c)^2 \end{bmatrix} = \begin{bmatrix} \bar{1} \\ 1 \\ t^2 \end{bmatrix} \tag{10}$$

For θ close to 90° (or c/a close to 1) this axis is close to $[\bar{1}11]$. Now the 4-domain junction highlighted in Figure 9 sits at the intersection of the boundary planes *ab* and *ad*. Written in the coordinate system of domain *a*, these two planes are (101) and something close to (110), and thus the intersection is close to $\pm[\bar{1}11]$. So, it is clear that the mismatch Θ rotates about an axis close to the <111> direction defining the 4-domain junction, or in other words, this constitutes a disclination of mismatch angle Θ along a direction close to the 4-domain junction line.

Now if we consider the real situation, then the formation of the domain structure results in a domain structure that would have corrugated ends at the junction if the two bands were separated, as shown in Figure 10 (as originally noted by Arlt and Sasko[2]). The band junction consists of forcing all the end planes to lay flat, with all the lattice curvature and stress that this entails. It is clear that if the 2:1 bimodal distribution of domain widths of Arlt is followed, then the *ad* boundary will take the lion's share of the tilt: 2Θ/3 about $[\bar{1}11]$ away from the ideal 180° misorientation. The remaining Θ/3 would be partitioned to the *bc* boundary.

In our measurements of the band junction in the BF-PT structure, the 90°-α values measured on either side of the band junction were ~83° and ~84.5°, respectively, corresponding to Θ values of 12.3° and 9.7°, respectively. In this context, the measured tilt of ~ 7.6° is definitely in the right region for 2Θ/3, and the measured tilt axis is within error limits of $[1\,\bar{1}\,\bar{1}]$. For the 90° domain boundary *bc*, the effect of the Θ/3 ≈ 4° rotation (about $[1\,\bar{1}\,1]$) on an ideal rotation of about 83 – 84.5° about $[\bar{1}\,00]$ would be to change the rotation angle to ~ 86°, whilst changing the axis very little, in excellent agreement with the measured *bc* misorientation of 86.2° about an axis close to <100>.

For the PZT, using the local c/a ratio measured from the misorientations at the "90°" domain boundaries of 1.021, Θ would be 2.1°. If the idealized 2:1 width ratio of domains were seen either side of the band junction, then the misorientation of the "180°" domains would be of the order of 2Θ/3, and we would expect a misorientation of about 1.4°. In fact, we see a misorientation closer to 1°, and if the orientation map is to be believed, the 180° domains, *a* and *d* are at least as wide as the 90° domains, and thus a misorientation of Θ/2 seems more reasonable, i.e. ~ 1°, which is in better accord with measured results. The remaining 1° of misorientation would then be partitioned to the "90°" boundary between *b* and *c* resulting in a misorientation of 89.4° about an axis very close to $[\bar{1}\,00]$, which agrees with experimental misorientation measurements of 89.50° ± 0.15° about an axis very close to $[\bar{1}\,00]$.

This information makes it possible to interpret the misorientations observed in broad beam EBSD maps such as those of Figures 2 and 5, as well as those published previously by Burnett *et al.*[10,16]. Such broad beam maps appear to pick up just one crystallographic orientation per lamellar colony; if we consider that each

EBSD pattern with a broad beam will contain contributions from both domains, but will be dominated by the wider of the two, i.e. domain *b* in the parlance of Figure 9. Similarly, a different lamellar colony in the same grain will have its EBSD pattern dominated by domain *c*. Thus, the broad beam EBSD maps will just show 90° domain boundaries at the band junctions. But, as has been shown above, these 90° domain boundaries will not have a misorientation given by $\theta = 2 \tan^{-1}(a/c)$ about <010>, but one that has been adjusted by a rotation of between $\Theta/3$ and $\Theta/2$ about <111> (where Θ is defined above). This all assumes that we are dealing with well-defined herringbone structures, as are observed in the single crystal BF-PT specimen. Thus the observation of bands separated by a misorientation of about 85° by EBSD maps of BF-PT taken with larger step sizes accords well with calculations for the bulk c/a ratio calculated from X-ray diffraction data of 1.13[14]; for this value we would expect $\theta \sim 83°$, $\Theta/3 \sim 4°$ and this would give a relative orientation across band junctions of 85.3°. The agreement is less good if we assume that the c/a ratio was 1.10, as suggested by powder X-ray diffraction from this sample[10]; and thus the EBSD results seem to suggest that the c/a ratio in the as-grown crystal is generally closer to 1.13 than 1.10. Further EBSD studies of the misorientations between neighbouring domains would help to clarify the local c/a ratios in the single crystal as discussed in our previous publication[12], but it is possible that the structure may have been altered by the grinding process used in the powder preparation for X-ray diffraction. Thus, in the well-ordered herringbone structures, information about the precise width ratio of the 90° and 180° domains, together with the measured deviation from 90° at the band junctions gives information on Θ, allowing us to derive θ and therefore the local c/a ratio.

In the case of the much finer-grained PZT, the junctions between bands are often less regular, as is clear in Figure 5, and although herringbone-type junctions are observed (e.g. Figs 6, 7 and 8), other forms of domain junctions are clearly also present. In such an irregular structure, it would therefore be dangerous to attempt to gain any information about c/a ratios from angles at the band junctions, and we have consequently not attempted any further analysis of the large step size orientation data of Fig.6 to determine information about the c/a ratios.

B. Strain estimation at the junctions

It is clear from the orientation maps presented that the areas very close to the band junctions are highly strained; pattern quality maps are superimposed on the boundary maps of Figures 3c, 7b and 8a, and show dark areas at the band junctions. Such dark areas correspond to regions of high strain and lattice rotation leading to the formation of significant overlaps / band diffuseness in the EBSD pattern. Attempts have been made in the metallurgical literature to relate such measures of pattern diffuseness to plastic strain, but not always with complete success. From our point of view, we shall make no attempt to use this information in a quantitative manner, but just point out that it clearly shows localised strain at the junctions. The dark areas at the junction also correspond well to the region showing the most localised lattice rotation in the analysis of Figure 8.

From the data presented in this paper, it is impossible to determine in a completely rigorous manner the strain tensor for points around the band junctions, although some analysis can be used to reveal key features of the strain. If we treat the problem as one of simple bending around the disclinations that describe the angular

mismatch between the rotations at the different domain boundaries, then we can calculate the peak tensile strain. This will occur at the four-domain boundary *ab'c'd* at a distance of half the 180° domain width from the centre (at which point the strain should be zero, if we are to balance total strain over the whole junction to zero). The amount of crystalline rotation in the PZT example of Figure 8 is about 1° (0.017 rad), this rotation occurs over about 60 nm and the domain width is about 100 nm, so bending happens with a radius of about 50 nm. Thus the strain is given by:

$$\varepsilon = \frac{\Delta l}{l} = \frac{w\eta}{2l} \tag{11}$$

where η is the lattice rotation. So in this case ε = 0.7 %. Using the published Young's modulus of PZT of 80 GPa[17], this equates to a tensile stress of 0.56 GPa. This is a rather lower figure than that estimated rather qualitatively by MacLaren *et al.*[1] based purely on image contrast rather than on explicit measurements of tilting across a boundary, and this shows the importance of using orientation mapping for evaluating this stress concentrations in detail.

For the BF-PT, we do not have such accurate measures of how quickly the tilt is achieved over the boundary, since the orientation map was recorded with a larger step size of 80 nm. It is, nevertheless, possible to make a crude estimate of the peak tensile stress and strain using the above approach. The rotation from one domain to the other appears to be complete over two hexagons of the map, i.e. l = 160 nm, the angle of tilt was measured above as 7.6°, and the width of the domains in the map appears to be of the order of 80 nm. This gives a peak strain of 3.3 %. There are no published measurements of the Young's modulus of BF-PT of exactly this composition, although it has been measured as 43 GPa for $(BiFeO_3)_{0.65}(PbTiO_3)_{0.35}$[18], assuming a similar value here would give a peak stress of ~1.4 GPa.

In both materials, very high stresses appear to be concentrated at the band junctions. Nevertheless, the theoretical strength of ionic materials (in order to cause failure by rupture of the atomic bonds) is generally thought to be of the order of 0.1E (where is the Young's modulus), equivalent to a tensile elastic strain of 0.1. So, although high strains and stress are present at the band junctions, these are unlikely to be sufficient to cause spontaneous rupture and initiate microcracking, without some additional factors being present to further concentrate the stress at a given point. Of course, once a crack has been initiated in such a material, it will interact with these stress concentrations at the band junctions and is likely to propagate very easily along this junction, as is, for instance, clearly shown in Figure 1a.

In order to gain a more accurate local picture of the stresses at such junctions, a number of steps would need to be taken. Firstly, the best orientation for observing the junction would be along the near-<111> orientation that defines the 4-domain junctions and the mismatch axes, since then each point in the orientation map would only sample a single orientation, and not get a superposition of different orientations. Secondly, the method used by commercial orientation mapping software involving determining each orientation individually and then calculating misorientations from this is well known to result in significant orientation noise in the misorientations, and this restricts our ability to accurately measure small misorientations; the alternative method using direct measurement of pattern shifts with a cross-correlation approach[19] may have more promise here. Finally, a higher spatial resolution than is available with the experimental measurements made in this work would be desirable to examine the rapidly varying strain fields in the vicinity of such junctions in more detail; one solution would be to further develop TEM Kikuchi pattern based methods to allow higher lateral resolution orientation mapping.

V. CONCLUSIONS

It has been shown that the junctions of lamellar bands in herringbone domain structures in two different tetragonal perovskite materials, lead zirconate titanate and bismuth ferrite – lead titanate, can be studied using electron backscatter diffraction – based crystallographic orientation mapping. This allows the resolution of the lamellar domain structure to either side of the band junction, together with information about the lattice rotation at the junction itself. The lattice rotations at these band junctions have been compared with crystallographic models of the structure of such junctions and the experimental data agrees extremely well with predictions. In one junction in PZT, the lattice rotation across the 180° domain was examined in detail and a lattice rotation of about 1° in about 55-70 nm was recorded. This was used in a simple model to evaluate the peak stress in this junction and a value of 0.56 GPa was estimated. It was not possible from the data to evaluate a figure for the BF-PT with anything like the same accuracy, but it is clear that the stress is very high, at least in the range 1-2 GPa, in accordance with the large c/a ratio in this material and attendant large angular mismatches at the domain boundaries and band junctions in this material. Finally, consideration was given to experimental improvements which would allow a more detailed and more quantitative analysis of the stress and strain distribution in such junctions.

ACKNOWLEDGEMENTS

This work was made possible by research funding provided by the EPSRC (grant reference EP/D032768/1). RV is grateful to CONACYT, Mexico for the

provision of a PhD studentship. TLB would like to acknowledge the support of EPSRC and Goodrich Control Systems Ltd.. HK and MJH would like to thank the DFG for supporting their work on PZT ceramics via the collaborative research centre on "Electric Fatigue in Functional Materials" (SFB 595).

1. I. MacLaren, L.A. Schmitt, H. Fuess, H. Kungl, and M.J. Hoffmann, J. Appl. Phys., **97**, 094102 (2005).
2. G. Arlt and P. Sasko, J. Appl. Phys., **51**, 4956 (1980).
3. G. Arlt, J. Mater. Sci., **25**, 2655 (1990).
4. N.A. Pertsev and G. Arlt, Ferroelectrics, **123**, 27 (1991).
5. N.A. Pertsev and H. Arlt, Fizika Tverdogo Tela, **33**, 3077 (1991).
6. N.A. Pertsev and G. Arlt, Ferroelectrics, **132**, 27 (1992).
7. T. Mori, E.C. Oliver, M.R. Daymond, and P.J. Withers, J. Neutron Res., **12**, 39 (2004).
8. T.L. Burnett, T.P. Comyn, and A.J. Bell, J. Cryst. Growth, **285**, 156 (2005).
9. M. Hammer and M.J. Hoffmann, J. Am. Ceram. Soc., **81**, 3277 (1998).
10. T.L. Burnett, T.P. Comyn, E. Merson, and A.J. Bell, IEEE T. Ultrason. Ferr., (2008) *in press*.
11. P.S. Bate, R.D. Knutsen, I. Brough, and F.J. Humphreys, J. Microsc. (Oxford), **220**, 36 (2005).
12. M.U. Farooq, R. Villaurrutia, I. MacLaren, H. Kungl, M.J. Hoffmann, J.-J. Fundenberger, and E. Bouzy, J. Microsc. (Oxford), (2008) *in press*.
13. A. Godfrey, G.L. Wu, and Q. Liu, Textures of Materials - Materials Science Forum, **408-4**, pp. 221-226 (2002)
14. S.A. Fedulov, Yu.N. Venevtsev, G.S. Zhdanov, E.G. Smazhevskaya, and I.S. Rez, Kristallografiya, **7**, 77 (1962).
15. L.A. Schmitt, K.A. Schönau, R. Theissmann, H. Fuess, H. Kungl, and M.J. Hoffmann, J. Appl. Phys., **101**, 074107 (2007).
16. T.L. Burnett, T.P. Comyn, E. Merson, and A.J. Bell, proceedings of the 16th IEEE International Symposium on Applications of Ferroelectrics, pp. 395-397 (2007)
17. A. Jimenez and J.M. Vicente, J. Phys. D - Appl. Phys., **33**, 1525 (2000).

18. A.B. Kounga Njiwa, E. Aulbach, J. Rödel, S.L. Turner, T.P. Comyn, and A.J. Bell, J. Am. Ceram. Soc., **89**, 1761 (2006).
19. A.J. Wilkinson, G. Meaden, and D.J. Dingley, Mater. Sci. Tech., **22**, 1271 (2006).

Figure Captions

FIG. 1: Backscattered scanning electron microscope images of domain structures in BF-PT: a) Higher magnification image showing domains in a herringbone configuration, with a crack through the centre of the structure; b) larger area view showing just lamellar bands rather than the individual domains, and demonstrating that the band arrangement is highly regular, persisting over hundreds of microns.

FIG. 2: Low resolution EBSD orientation map showing the lamellar bands in the BF-PT structure – one orientation is primarily identified for each lamellar band.

FIG. 3: EBSD orientation data from a lamellar junction in the BFPT material: a) orientation map coloured according to b) the inverse pole figure; c) domain boundary map with boundaries coloured according to d) the boundary misorientation histogram.

FIG. 4: Secondary electron image of the domain structure of the 42.5/57.5 PZT sample (the sample has been lightly etched to give good domain contrast).

FIG. 5: Large step size EBSD data for a La-Sr-doped PZT 42.5/57.5: a) orientation map with colours according to the inverse pole figure key of Fig. 3b; b) boundary map with (domain) boundaries in the range of 87-93° coloured according to the misorientation histogram of c), with other (grain) boundaries indicated as black lines and overlaid on the image quality map; c) misorientation histogram for the range 87-90°.

FIG. 6: Secondary electron image of a lightly etched domain structure showing herringbone domain structures.

FIG. 7: EBSD mapping of a junction in the La-Sr doped PZT 42.5/57.5: a) orientation map with colours according to the inverse pole figure of Fig. 3b; b) boundary map with misorientations coloured according to the misorientation angle histogram of d); c) secondary electron image of the area mapped; d) misorientation angle histogram for the domain boundaries with misorientations in the range 87°-90°.

FIG. 8: Line scans of point-to-point and cumulative misorientations across the 180° domain boundaries in the area mapped in Fig. 7: a) Locations of the two line scans, red lines denote the 90° domain boundaries, yellow lines denote small angle boundaries in the range 0.5-1.2°; b) misorientation plotted against distance along the left hand green line; c) misorientation plotted against distance for the right hand green line.

FIG. 9: Schematic diagram of a 4-domain junction at band junction in a herringbone domain structure looking parallel to the [100] axis of domain *b*. Edge-on boundaries are indicated with a single heavy line, whereas inclined domain boundaries are indicated by a heavy line and two parallel narrow lines in the direction of inclination. The direction of viewing is parallel to the **a** direction in either domains *b* or *c*.

FIG. 10: Schematic diagram of the same domain structure looking along $[\bar{1}\,1\,\bar{1}]$ in domain *b* (close to $[\bar{1}\,11]$ in domain *a*). The domains are shown in the unstrained

form where the surfaces are released at the junction to follow their preferred orientations so as to see the mismatch angles clearly.

FIG. 1: Backscattered scanning electron microscope images of domain structures in BF-PT: a) Higher magnification image showing domains in a herringbone configuration, with a crack through the centre of the structure; b) larger area view showing just lamellar bands rather than the individual domains, and demonstrating that the band arrangement is highly regular, persisting over hundreds of microns.

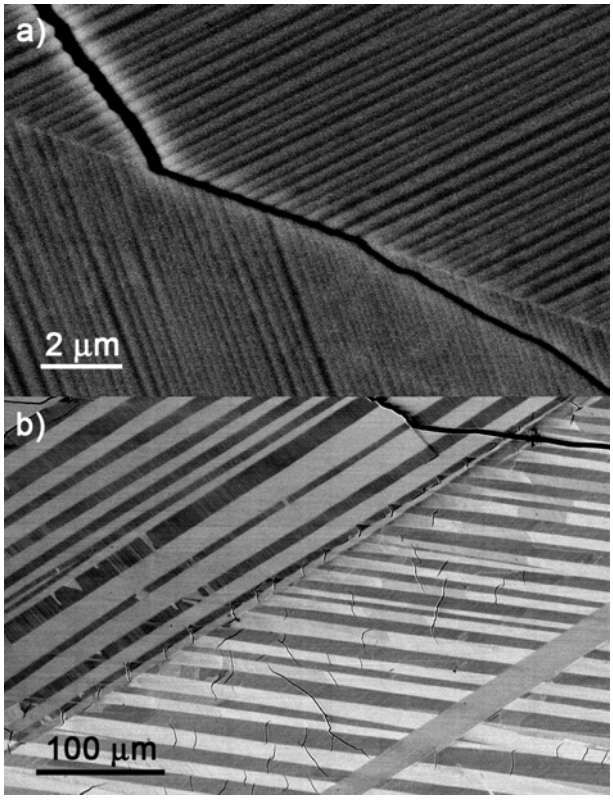

FIG. 2: Low resolution EBSD orientation map showing the lamellar bands in the BF-PT structure – one orientation is primarily identified for each lamellar band.

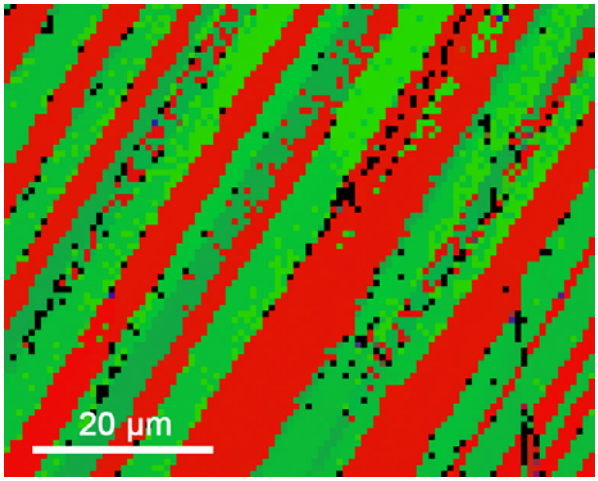

FIG. 3: EBSD orientation data from a lamellar junction in the BFPT material: a) orientation map coloured according to b) the inverse pole figure; c) domain boundary map with boundaries coloured according to d) the boundary misorientation histogram.

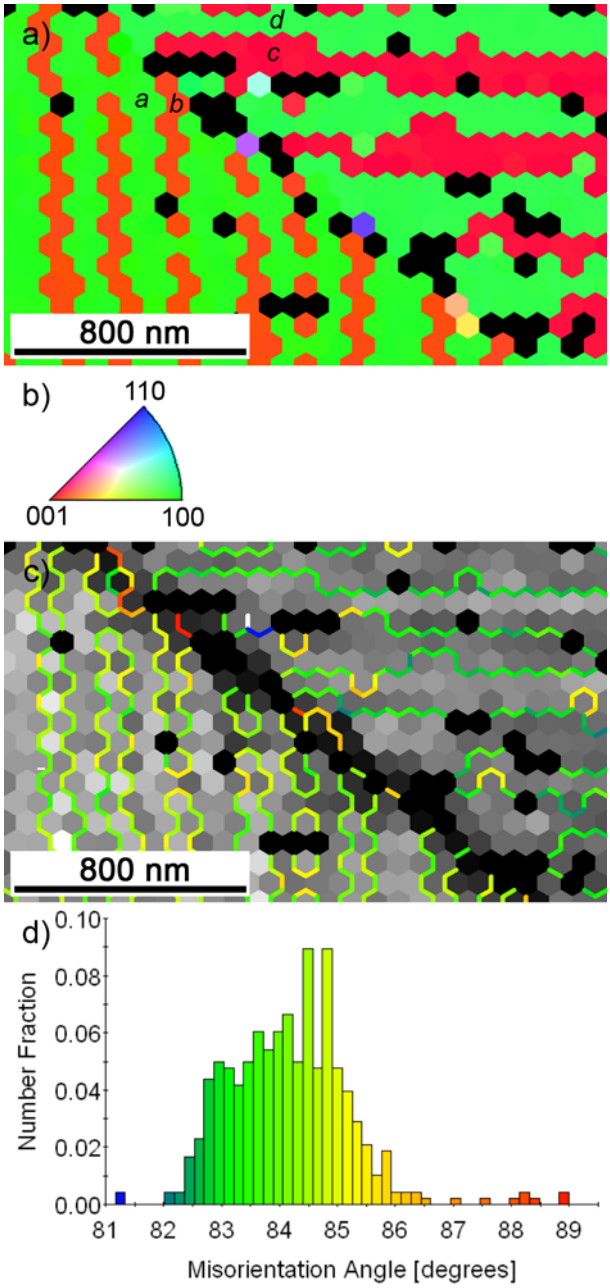

FIG. 4: Secondary electron image of the domain structure of the 42.5/57.5 PZT sample (the sample has been lightly etched to give good domain contrast).

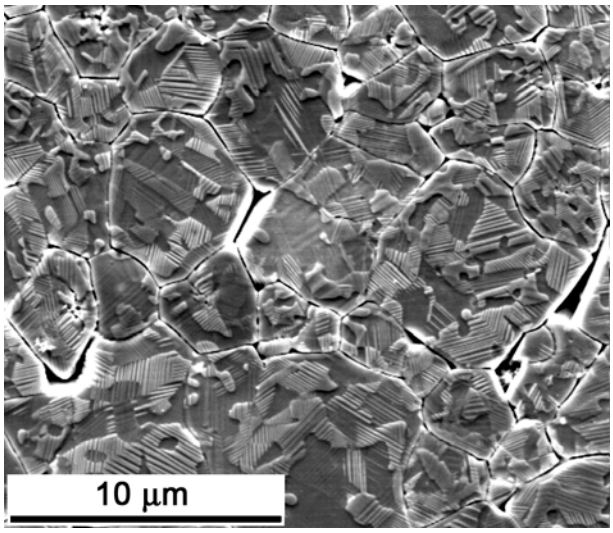

FIG. 5: Large step size EBSD data for a La-Sr-doped PZT 42.5/57.5: a) orientation map with colours according to the inverse pole figure key of Fig. 3b; b) boundary map with (domain) boundaries in the range of 87-93° coloured according to the misorientation histogram of c), with other (grain) boundaries indicated as black lines and overlaid on the image quality map; c) misorientation histogram for the range 87-90°.

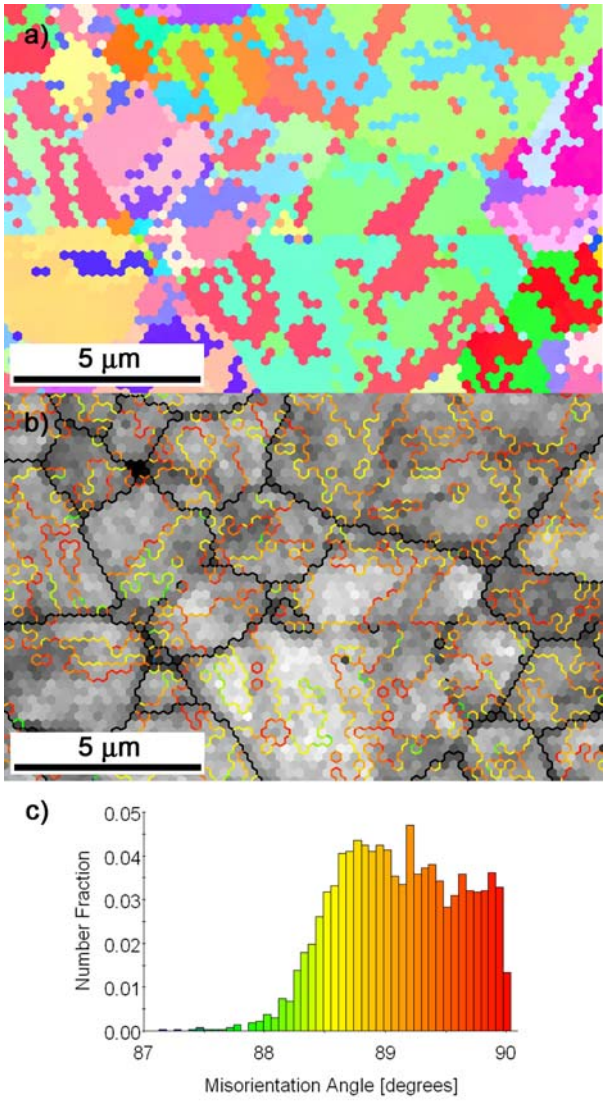

FIG. 6: SE image of a lightly etched domain structure showing herringbone domain structures.

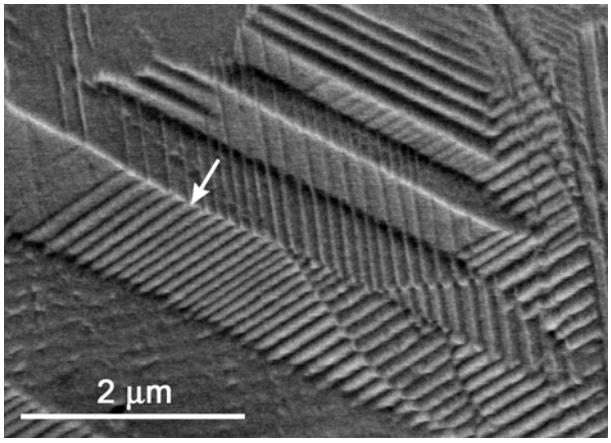

FIG. 7: EBSD mapping of a junction in the La-Sr doped PZT 42.5/57.5: a) orientation map with colours according to the inverse pole figure of Fig. 3b; b) boundary map with misorientations coloured according to the misorientation angle histogram of d); c) secondary electron image of the area mapped; d) misorientation angle histogram for the domain boundaries with misorientations in the range 87°-90°.

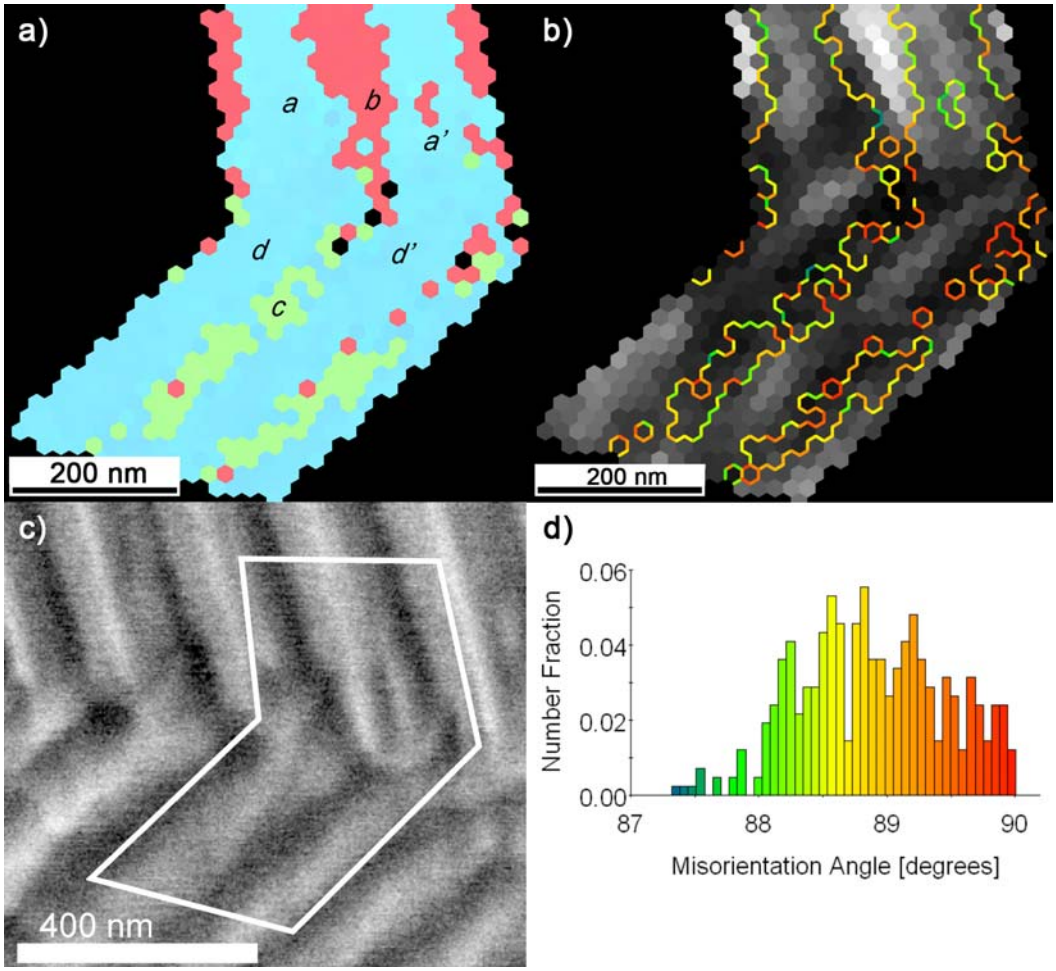

FIG. 8: Line scans of point-to-point and cumulative misorientations across the 180° domain boundaries in the area mapped in Fig. 7: a) Locations of the two line scans, red lines denote the 90° domain boundaries, yellow lines denote small angle boundaries in the range 0.5-1.2°; b) misorientation plotted against distance along the left hand green line; c) misorientation plotted against distance for the right hand green line.

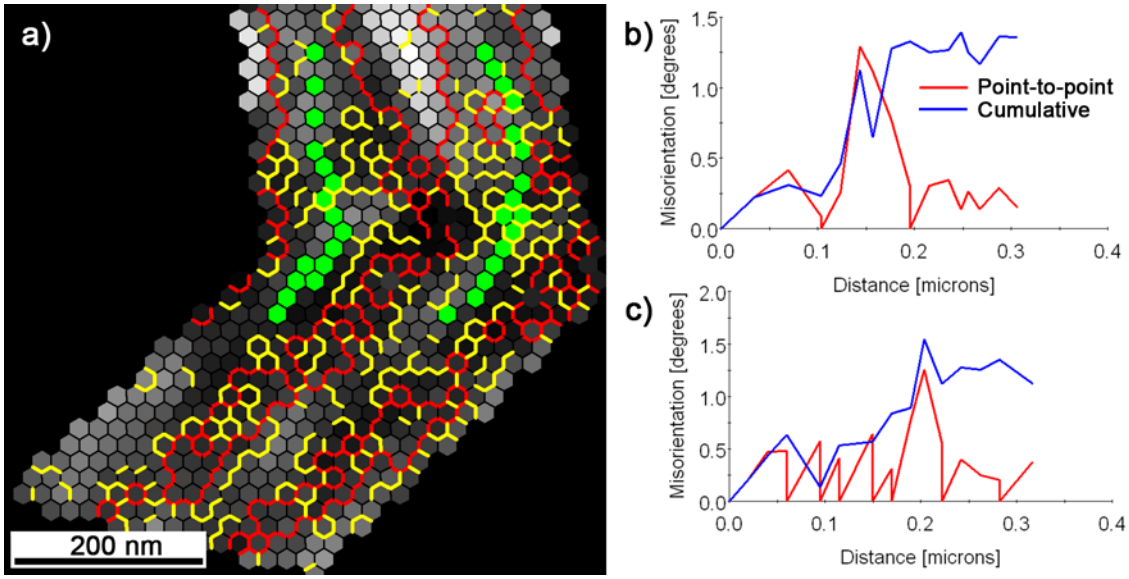

FIG. 9: Schematic diagram of a 4-domain junction at band junction in a herringbone domain structure looking parallel to the [100] axis of domain *b*. Edge-on boundaries are indicated with a single heavy line, whereas inclined domain boundaries are indicated by a heavy line and two parallel narrow lines in the direction of inclination. The direction of viewing is parallel to the **a** direction in either domains *b* or *c*.

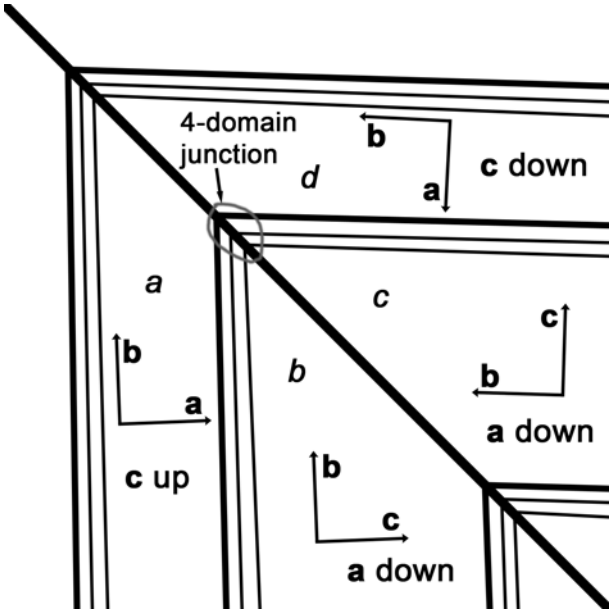

FIG. 10: Schematic diagram of the same domain structure looking along $[\bar{1}1\bar{1}]$ in domain *b* (close to $[\bar{1}11]$ in domain *a*). The domains are shown in the unstrained form where the surfaces are released at the junction to follow their preferred orientations so as to see the mismatch angles clearly.